Paper
Int'l J. of Aeronautical & Space Sci. 18(1), 48–55 (2017)
DOI: doi.org/10.5139/IJASS.2017.18.1.48

IJASS
International Journal of Aeronautical and Space Sciences

On the computation of low-subsonic turbulent pipe flow noise with a hybrid LES/LPCE method

Seungtae Hwang* and Young J. Moon**

Computational Fluid Dynamics and Acoustics Laboratory, School of Mechanical Engineering, Korea University, Seoul 02841, Republic of Korea

Abstract

Aeroacoustic computation of a fully-developed turbulent pipe flow at Re_τ = 175 and M = 0.1 is conducted by LES/LPCE hybrid method. The generation and propagation of acoustic waves are computed by solving the linearized perturbed compressible equations (LPCE), with acoustic source DP(x,t)/Dt attained by the incompressible large eddy simulation (LES). The computed acoustic power spectral density is closely compared with the wall shear-stress dipole source of a turbulent channel flow at Re_τ = 175. A constant decaying rate of the acoustic power spectrum, $f^{-8/5}$ is found to be related to the turbulent bursts of the correlated longitudinal structures such as hairpin vortex and their merged structures (or hairpin packets). The power spectra of the streamwise velocity fluctuations across the turbulent boundary layer indicate that the most intensive noise at $\omega^+ < 0.1$ is produced in the buffer layer with fluctuations of the longitudinal structures ($k_zR < 1.5$).

Key words: Low-subsonic, Turbulent pipe flow noise, Computational aeroacoustics, Turbulent bursts

1. Introduction

While many research groups have addressed the exterior noise issues posed by aircrafts during take-off and landing, e.g. trailing-edge noise, slat noise, landing gear noise, etc., insufficient efforts have been made to understand and reduce the aerodynamic noise generated by the aircraft internal cooling and ventilation systems (called ECS for Environmental Control System). Many interactions take place between sub-components of a given ECS: the blower unit, temperature and pressure regulating devices, or simply duct connections, and ECS is indeed a contributor to the noise perceived by passengers and crew within the cabin and cockpit. For example, interior noise induced by ECS exceeds the other noise sources such as external turbulent boundary layer, or electronic equipment(e/e) cooling in the most disturbing frequency range, 100 Hz < f < 1000 Hz. In fact, ECS noise exhibits a tonal broaden peak, 15 - 25 dB higher than the others at f = 300 Hz[1].

In the present study, we are interested in computational modeling and understanding in detail the noise generating mechanisms of low-subsonic, turbulent flow in the ventilation pipe, the most basic unit of ECS. The noise produced by turbulent boundary layer (called TBL from hereafter) has been an important issue in turbulent flow research for more than fifty years. It is generally known that the TBL noise is generated indeed by convecting near-wall turbulences. The TBL noise is either emitted into ambient air, or transmitted through the walls via (i) acoustic loading and (ii) pressure fluctuations at the wall surface. Note that the energy level of the acoustic loading is much lower but its transmission can be comparable when a transfer function is considered.

The TBL noise transmission is often concerned at low wavenumbers because it is more likely to interact with structures by resonance effect. On the low-wavenumber acoustics, a few but very intensive theoretical studies have been conducted since 1950's; the Kraichnan-Phillips theorem asserted that the wall pressure fluctuation spectrum converges to zero in a sub-convective region (i.e. axial wavenumber is less than ω/U_∞ but still larger than ω/c). Ffowcs-williams[2]

* Ph. D candidate
** Professor, Corresponding author: yjmoon@korea.ac.kr

Received: Demcember 29, 2016 Revised: February 13, 2017 Accepted: February 15, 2017

http://ijass.org pISSN: 2093-274x eISSN: 2093-2480

showed later in his theoretical work that the spectral level of wall pressure fluctuation at the sub-convective and acoustic regimes must have a finite non-zero value, with the compressibility effect included in the analysis.

Along the line, Arguillat et al.[3] measured the wall pressure fluctuations in a turbulent channel flow at low Mach numbers and showed that when the noise transmission is included in the analysis, not only the aerodynamic loading by hydrodynamic pressure but also the effect of the low wavenumber (acoustic part) have to be taken into account. Hu et al.[4] also attempted to quantify the noise sources in the turbulent channel flow with incompressible direct numerical simulation (DNS) and predicted the acoustic pressure fluctuations at low Mach numbers with the Lighthill's acoustic analogy. They found that the acoustic pressure fluctuation of the dipole source is more dominant below a specific Mach number (e.g. M < 0.1).

In the present study, aeroacoustic computation of a fully-developed turbulent pipe flow is conducted at low Mach number. This task is computationally challenging since acoustic field is superimposed on the flow field within the pipe. An LES/LPCE hybrid method is thereby used to solve the hydrodynamic field and acoustic field separately with different grid systems. An incompressible large-eddy simulation (LES) is conducted for a fully developed turbulent flow at Re_τ = 175, employing a computational domain of 22 pipe-diameters in length. The acoustic field inside the pipe is computed at M = 0.1 by solving the linearized perturbed compressible equation (LPCE), with acoustic source DP/Dt acquired from the incompressible LES solution. The computational acoustic grid is elaborately arranged such that turbulent flow field with acoustic source can be filtered in the acoustic monitoring zones. A duct mode and acoustic power spectrum of the turbulent pipe flow noise are analyzed and discussed along with an acoustic source model proposed by Morfey[5], i.e. the wall shear-stress fluctuation acoustic dipole. To investigate the noise sources, the spectral characteristics of the axial velocity fluctuations are examined across the turbulent boundary layer.

This paper is organized as follows. In Sec. II, the computational methodologies are described. The results and discussion of hydrodynamics and acoustics of turbulent pipe flow follow in Sec. III and IV. Finally, the paper provides the conclusion.

2. LES/LPCE Hybrid Formulation

The present LES/LPCE hybrid method is based on a hydrodynamic/acoustic splitting method(Hardin et al.[6]), in which the total flow variables are decomposed into the incompressible and perturbed compressible variables as,

$$\begin{aligned} \rho(\vec{x},t) &= \rho_0 + \rho'(\vec{x},t) \\ \vec{u}(\vec{x},t) &= \vec{U}(\vec{x},t) + \vec{u}'(\vec{x},t) \\ p(\vec{x},t) &= P(\vec{x},t) + p'(\vec{x},t) \end{aligned} \tag{1}$$

The incompressible variables represent the hydrodynamic flow field, while the acoustic fluctuations and other compressibility effects are resolved by the perturbed quantities denoted by (').

The hydrodynamic turbulent flow field is first solved by incompressible LES. The filtered incompressible Navier-Stokes equations are written as,

$$\frac{\partial \tilde{U}_j}{\partial x_j} = 0 \tag{2}$$

$$\begin{aligned} &\rho_0 \frac{\partial \tilde{U}_i}{\partial t} + \rho_0 \frac{\partial}{\partial x_j}\left(\tilde{U}_i \tilde{U}_j\right) \\ &\quad = -\frac{\partial \tilde{P}}{\partial x_i} + \mu_0 \frac{\partial}{\partial x_j}\left(\frac{\partial \tilde{U}_i}{\partial x_j} + \frac{\partial \tilde{U}_j}{\partial x_i}\right) - \rho_0 \frac{\partial}{\partial x_j} M_{ij} \end{aligned} \tag{3}$$

where the grid-resolved quantities are denoted by (˜) and the unknown sub-grid tensor M_{ij} is modeled as

$$M_{ij} = \widetilde{U_i U_j} - \tilde{U}_i \tilde{U}_j = -2(C_s \Delta)^2 |\tilde{S}| \tilde{S}_{ij} \tag{4}$$

Here, Δ is the mean radius of the grid cells (computed as cubic root of its volume), and $\tilde{S}_{ij}$ is the strain-rate tensor.

After a quasi-periodic stage of the hydrodynamic field is attained, the perturbed quantities are computed by the linearized perturbed compressible equations (LPCE)(Seo and Moon[7]). A set of the linearized perturbed compressible equations is written as,

$$\frac{\partial \rho'}{\partial t} + \left(\vec{U} \cdot \nabla\right)\rho' + \rho_0 (\nabla \cdot \vec{u}') = 0 \tag{5}$$

$$\frac{\partial \vec{u}'}{\partial t} + \nabla\left(\vec{u}' \cdot \vec{U}\right) + \frac{1}{\rho_0}\nabla p' = 0 \tag{6}$$

$$\frac{\partial p'}{\partial t} + \left(\vec{U} \cdot \nabla\right)p' + \gamma P (\nabla \cdot \vec{u}') + (\vec{u}' \cdot \nabla)P = -\frac{DP}{Dt} \tag{7}$$

The left hand side of LPCE represents effects of acoustic wave propagation and refraction in an unsteady, inhomogeneous flow, while the right hand side only contains an explicit acoustic source component, which is projected from the incompressible LES flow solution. It is interesting to note that for low Mach number flows, the total derivative of the hydrodynamic pressure, DP/Dt is only considered as the explicit noise source term. From the curl of linearized perturbed momentum equations, Eq.(6) yields

$$\frac{\partial \vec{\omega}'}{\partial t} = 0 \tag{8}$$

The LPCE prevents any further changes(generation, convection and decaying) of perturbed vorticity in time, in

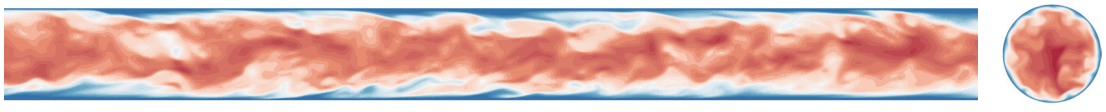

(a) (b)

Fig. 1. A fully-developed turbulent pipe flow at Re_D = 5000 (or Re_τ = 175); streamwise velocity u_z, showing only the first half of the computational domain 0 ≤ z ≤ 11D, (a) θ-constant plane and (b) z-constant plane.

fact, the perturbed vorticity could generate self-excited errors if ω' is not properly resolved with the acoustic grid. Hence, the evolution of the perturbed vorticity is pre-suppressed in LPCE, deliberating the fact that the perturbed vorticity has little effects on noise generation, particularly at low Mach numbers. For the hybrid method, this is an important property that ensures consistent, grid-independent acoustic solutions. Derivation of LPCE and the detailed discussion on characteristics of the perturbed vorticity can be found in Seo and Moon[7].

The filtered incompressible Navier-Stokes equations are solved by an iterative fractional-step method(Poisson equation for the pressure), wheras the linearized perturbed compressible equations are solved in a time marching fashion. To avoid excessive numerical dissipations and dispersions errors, the governing equations are spatially discretized with a sixth-order compact finite difference scheme(Lele[8]) and integrated in time by a four-stage Runge-Kutta method.

Practically, when a high order scheme is applied to stretched meshes, numerical instability is encountered due to numerical truncations or failure of capturing high wave-number phenomena. Thus, a tenth-order spatial filtering(cut-off wavenumber, $k\Delta x \approx 2.9$) proposed by Gaitonde et al.[9] is applied to every iteration to suppress the high frequency errors that might be caused by grid non-uniformity. For the far-field boundary condition, the energy transfer and annihilation (ETA) boundary condition(Edgar et al.[10]) with a buffer zone is used for eliminating any reflection of the out-going waves. The ETA boundary condition is easily facilitated with a rapid grid stretching in the buffer-zone and spatial filtering which damp out waves shorter than grid spacing. Therefore, if the buffer-zone has a grid spacing larger than the outgoing acoustic wave length, the wave can be successfully absorbed by the ETA boundary condition.

3. Large Eddy Simulation of Turbulent Pipe Flow

3.1 Computational modeling of turbulence scales

A fully-developed turbulent pipe flow is computed by incompressible large-eddy simulation for the friction Reynolds number (also known as Karman number), $Re_\tau = R^+ = u_\tau R/\nu = 175$ (or $Re_D = 5000$). For the computation of fully-developed turbulent pipe flow, a periodic boundary condition is to be used in the streamwise direction but one has to mind whether the computational domain is long enough to include the very large and large scale motions (called VLSM and LSM for short). These structures, initially observed in the experimental studies (Kim and Adrian[11] and Townsend[12]), are of 2-3R to 20R in length (R is the pipe radius) in the outer region of the turbulent boundary layer. Along the line, Chin et al.[13] conducted a DNS study at Re_τ = 170 and 500 to investigate the effect of the streamwise periodic length on the convergence of turbulence statistics and concluded that a streamwise domain length of convergence can be achieved with 8πR.

In the present study, we compute not only the turbulent pipe flow but also an acoustic field inside the pipe, i.e. generation and propagation of sound in the turbulent pipe flow. Therefore, the computational domain is set as 44R, large enough to analyze the flow and acoustics at the same time. The grid size is 120 × 241 × 1560 (about 45 millions) along r, θ, and z directions, respectively. The grid resolution in the axial direction is $\Delta z^+ = 5.5$ (or $\Delta z = 0.016$), and along the azimuthal direction, the maximum grid spacing at the pipe wall is $R\Delta\theta^+ = 4.5$ (or $R\Delta\theta = 0.013$). The minimum and maximum wall-normal grid spacings are $\Delta r^+ = 0.35$ and 2.8 (or $\Delta r = 0.001$ and 0.008), respectively. A time step, $\Delta t^+ = 0.017$ (or $\Delta t = 0.0007$) is used in the present LES, and the total simulation time is about $126R/U_\infty$. The computation was conducted with 600 processors of SUN B6275.

Figure 1 shows the computed fully-developed turbulent pipe flow with the flooded contours of the instantaneous streamwise velocity at a θ-constant plane and at a z-constant plane, respectively. A total of 30 contour levels are used to represent the magnitude of u_z from 0.004 (blue) to 1.4 (red), and the turbulent eddy structures in the pipe are well depicted by the present computation.

3.2 Validation of turbulence statistics

The present LES solution is validated by comparing with the existing DNS solutions of Khoury et al.[14], who studied

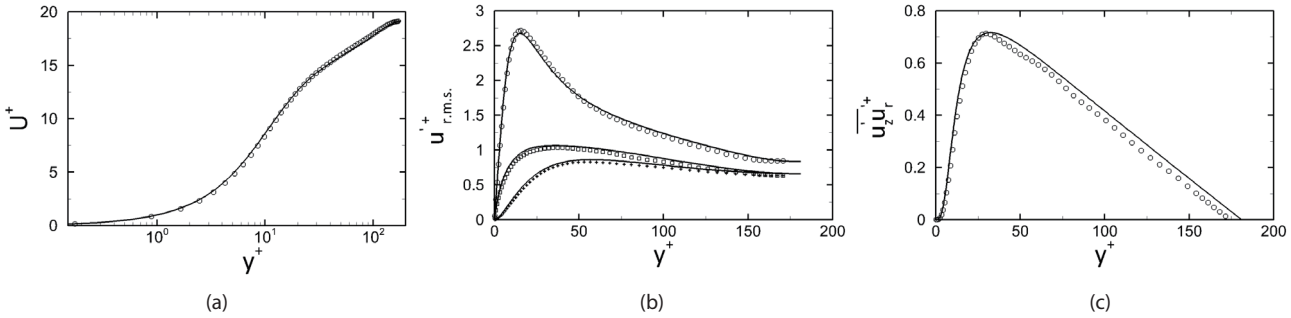

Fig. 2. (a) Mean axial velocity U^+ as a function of y^+. circles: present LES at Re_D = 5000; solid line: Khoury et al.[14] at Re_D = 5300., (b) Turbulence intensity u^+_{rms} vs. y^+; present LES(Re_D = 5000): $u^+_{z,rms}$(circle), $u^+_{\theta,rms}$(square), $u^+_{r,rms}$(cross); Khoury et al.[14]: line (Re_D = 5300), (c) turbulent shear stress $\overline{u'_z u'_r}^+$ vs. y^+; present LES: circle; Khoury et al.[14]: line.

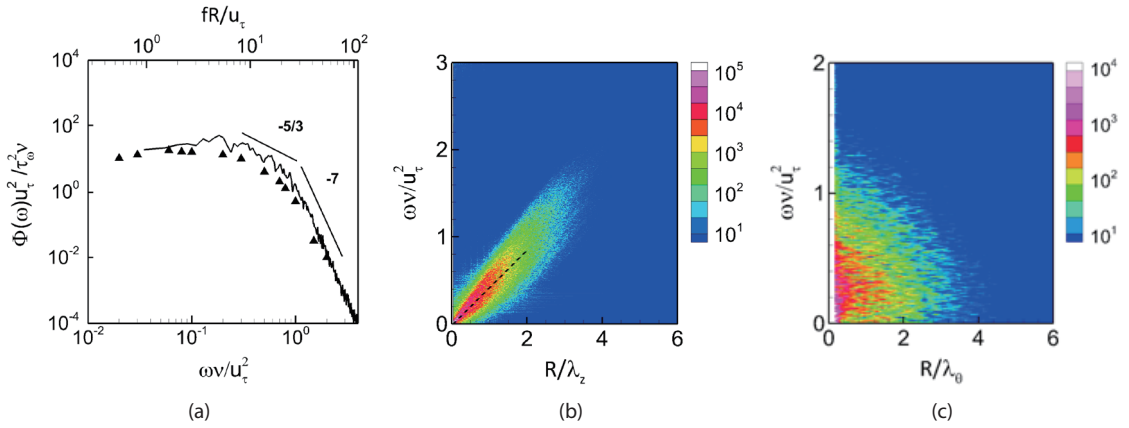

Fig. 3. (a) Power spectral density of wall pressure fluctuations. solid line: present LES; ▲: Gloerfelt and Berland (Re_θ = 1491)[15]; (b) cross-spectral contours of wavelength-frequency spectrum $\Phi(k_z,0,f)$ (left) and $\Phi(0,k_\theta,f)$ (right) of the wall pressure fluctuation. The dashed line in $\Phi(k_z,0,f)$ indicates a major correlation stream, $U_c = 0.8U_\infty$.

the characteristics of turbulent pipe flow in a smooth circular pipe of axial length 25R at Re_D = 5300. The inner-scaled mean velocity profile of the present calculation is compared in Fig. 2(a), and the three components of turbulence intensity, $u'_{z,rms}$, $u'_{\theta,rms}$, $u'_{r,rms}$ are compared in Fig. 2(b). Both comparisons indicate excellent agreement with DNS. Fig. 2(c) shows that a second-order turbulence statistics, turbulent shear stress is also closely compared with the DNS solution.

A power spectral density of hydrodynamic wall pressure fluctuation (scaled with inner flow variable) is presented in Fig. 3(a), comparing with that of Gloerfelt and Berland[15] (a subsonic turbulent boundary layer over a flat plate at Re_θ = 1491 and M = 0.5). The hydrodynamic wall pressure fluctuations seem to show similar spectral characteristics of the near-wall turbulences for both internal and external turbulent boundary layers. It is also noticeable that the spectral profile of the wall pressure fluctuation is almost plateau at frequencies below the inertial subrange. It should be noted that the local wall pressure fluctuations by near-wall motions of turbulence, LSM, in particular leave 'footprint' of the energetic motions close to the wall. To correlate with acoustic sources, it is important to know the spatio-temporal scales of turbulence, based on their footprints on the wall. $\Phi(k_z,k_\theta f)$, the wavenumber frequency spectra of wall pressure p(z,θ,t) are defined by a Fourier transform of space-time correlation functions,

$$R_{pp} = < p(z,\theta,t)p(z+\xi,\theta+\eta,t+\tau) > \quad (9)$$

Figure 3(b) shows the cross-spectra of wall pressure fluctuation along the flow axial (left) and azimuthal (right) directions. The x-axis shows the wavelength nondimensionalized by the pipe radius and y-axis indicates the frequency nondimensionalized by the inner scaling. It is observed that there is a clear trend of k_zR - ω^+ relation, showing a convection speed equal to $U_c = 0.8U_\infty$. The wall pressure fluctuation of flow axial direction seems to be energetic in the region where the turbulent eddy length exceeds the pipe radius. In particular, the spectral contribution of wall pressure fluctuation is effective for which the length scale is larger than 2R, similar to LSM structures. As to the VLSM

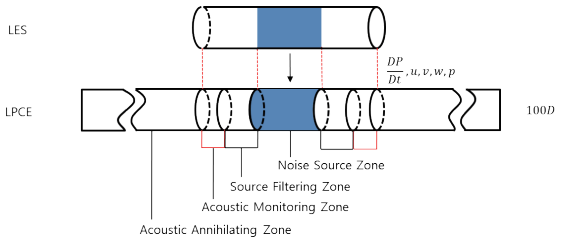

Fig. 4. Schematic figure of turbulent pipe flow noise prediction method.

structure, a recent DNS study of Chin et al.[13] reported with a similar flow condition that the formation of VLSM structure was hard to be observed in low Reynolds number flow. In the wall pressure cross-spectra, the azimuthal direction shows rather a monotonic result in comparison with the flow axial direction. The spectral contribution in the half pipe perimeter (0.5πD) is shown to be energetic than other regions for all frequencies.

4. Aeroacoustic Computation of Turbulent Pipe Flow

4.1 LPCE computation with acoustic source DP/Dt field

An elaborate methodology is used to compute the acoustic field of full-developed turbulent pipe flow at low Mach numbers. Once a fully-developed turbulent pipe flow is developed with incompressible LES, the linearized perturbed compressible equation (LPCE) is calculated with acoustic source DP/Dt. In LPCE computation, a total derivative of the hydrodynamic pressure fluctuations, DP/Dt, is only considered as an explicit volumetric source field[7].

Two different computational domains are configured as in Fig. 4, to separate the incompressible LES and LPCE computations. One important aspect in acoustic computation of the turbulent pipe flow is that a streamwise periodic boundary condition used for incompressible LES cannot be used for LPCE computation. It is to be noted that the acoustic solution is always superimposed with the turbulent flow fluctuations so that we cannot isolate acoustic field produced by turbulent fluctuations inside the pipe. For this, the computational grid for LPCE requires additional domains for source filtering, data collection, and wave annihilation.

The source filtering zone eliminates fluctuating acoustic sources such as velocities and hydrodynamic pressure. Sampling of temporal as well as spatial evolutions of acoustic waves are conducted in the acoustic monitoring zone. The acoustic annihilation zone at the side of the computational

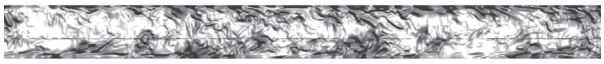

Fig. 5. A shadow view of instantaneous acoustic source field, DP/Dt at a θ-constant plane in turbulent pipe flow at $Re_\tau = 175$.

domain prevents unnecessary wave reflections; 50 grids points are stretched over 100D in the axial direction. With arrangement of different zones with different purposes, we can indeed acquire pure acoustic pressure fluctuations generated by fully-developed turbulent pipe flow at low Mach number.

The noise sources within the pipe are visualized in Fig. 5 by the shadow view of DP/Dt attained by LES. It is interesting to observe that the DP/Dt field depicts quite closely the near-wall turbulent structures, i.e. hairpin eddies and their merges structures. In fact, convection of these time-dependent near-wall structures are the primary noise sources in the turbulent pipe flow. With these time-dependent convecting motions with the flow will compress or decompress the compressible flow inside the pipe. In fact, it was shown that the (DP/Dt)/P field represents indeed the (Dρ/Dt)/ρ field, i.e. a volumetric dilatation rate of the fluid[16].

4.2 Instantaneous acoustic fields and duct mode

The linearized perturbed compressible equation is solved for the prediction of sound in turbulent pipe flow, in conjunction with the incompressible LES. A shadow view of the compressibly-perturbed pressure fluctuations (p') at a θ-constant plane is presented in Fig. 6 to visualize the instantaneous compression and expansion of the waves in the turbulent pipe flow. Nine consecutive images with a time interval of $\Delta t = 0.14D/U_\infty$ show not only the near-field hydrodynamic pressure fluctuations by turbulences but also the spatial formation and propagation of the acoustic waves. One can clearly note that two noticeable acoustic waves propagate towards both ends of the computational domain inside the pipe and that the convection speed of the continuous field solutions corresponds to the speed of sound.

In a circular pipe, acoustic mode[17] is determined by a cut-off frequency of higher modes, $f_{m,n} = n_{m,n}c/(2\pi R)$ where $n_{m,n}$ calculated from the Helmholtz equation denotes a number of nodal lines in the radial and azimuthal directions, respectively, with c being the speed of sound and R the pipe radius. For the computed acoustic field, acoustic mode is therefore checked to see the evanescence of the acoustic waves at the far field. The higher acoustic modes can be checked by phase angles at a cross-section of the pipe. Using the time evolution of acoustic pressure from a plane in the acoustic monitoring zone, the phase analysis

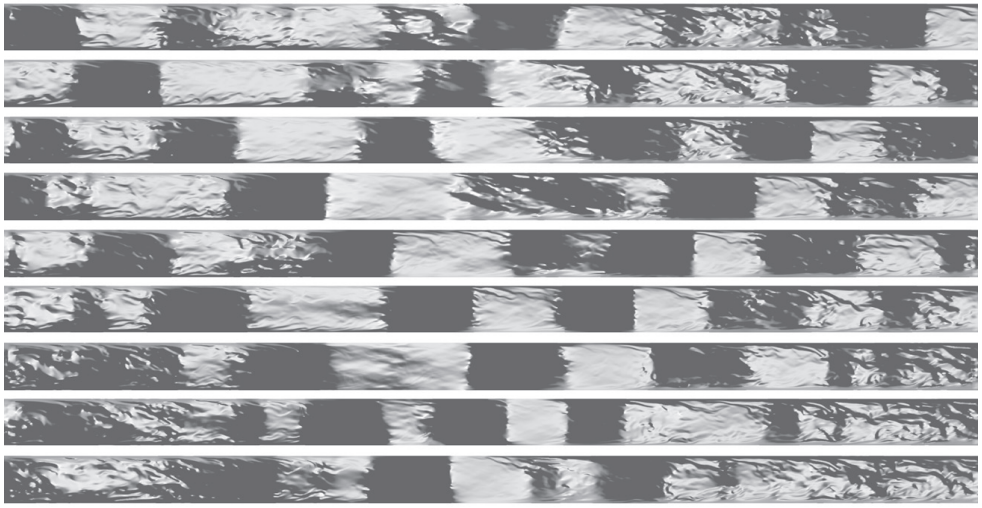

Fig. 6. Instantaneous snapshots of the compressibly-perturbed pressure fluctuation field p' at a θ-constant plane in the turbulent pipe flow at $Re_D = 5000$ (or $Re_\tau = 175$); $\Delta t = 0.14D/U_\infty$.

is conducted with equally-distributed 30 points in both radial and azimuthal directions. As presented in Fig. 7, a non-zero phase angle is only visible at the frequency close to 1.55 in terms of inner variables, and it is indeed close to the analytical cut-off frequency of (1,0) mode, that is, 1.6. In other words, there is no clear tendency of an additional acoustic mode at higher frequency, implying that the (1,0) mode is only observed in the present study. The phase angles near the (1,0) cut-off frequency range from - 90 ~ 90 degrees, with maximum and minimum at the pipe circumference. This is consistent with a representative characteristic of the acoustic higher mode, known as the spiral wave motion. There is, however, no clear higher acoustic modes, implying that acoustic waves at higher frequencies are expected to be either quickly damped by decaying characteristics of the small-scale turbulences or evanescence of waves during transmission in the pipe.

4.3 Spectral characteristics of acoustic field in turbulent pipe flow

A power spectral density of acoustic pressure computed by the present method is compared in Fig. 8 with the acoustic dipole source (marked by ▲) attained by Hu et al.[4], who conducted an incompressible DNS for a turbulent channel flow at Re_τ = 180. The axial dipole source (S11) spectrum of Hu et al[4]. scaled by $(S_p(f)Re_\tau)$ shows a good agreement with the present LES/LPCE acoustic result from low to mid-range frequencies ($1 < fR/u_\tau < 10$ or $0.04 < \omega^+ < 0.4$). As pointed out by Hu et al.[4], the TBL noise generation at low Mach number (e.g. M < 0.1) is majorly attributed to the linear mode conversion from incident vorticity wave to the pressure wave near the solid boundary. This noise generation mechanism was initially mentioned by Herbert, Leehay and

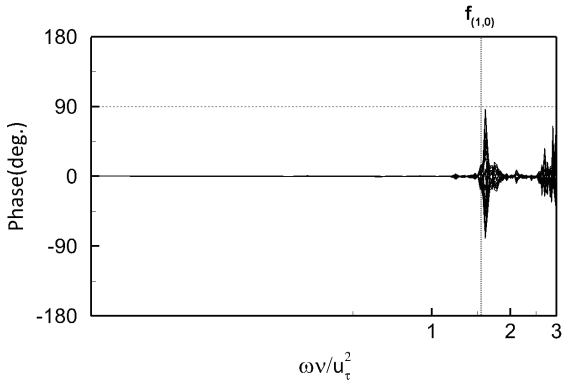

Fig. 7. Phase angle analysis. solid line: present LES; dashed line: analytic (1,0) duct mode frequency.

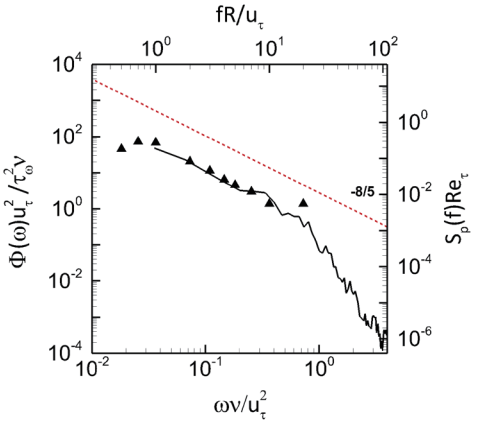

Fig. 8. Acoustic pressure power spectrum. solid line: present LES; ▲: axial dipole source (S_{11}, Hu et al.[4]).

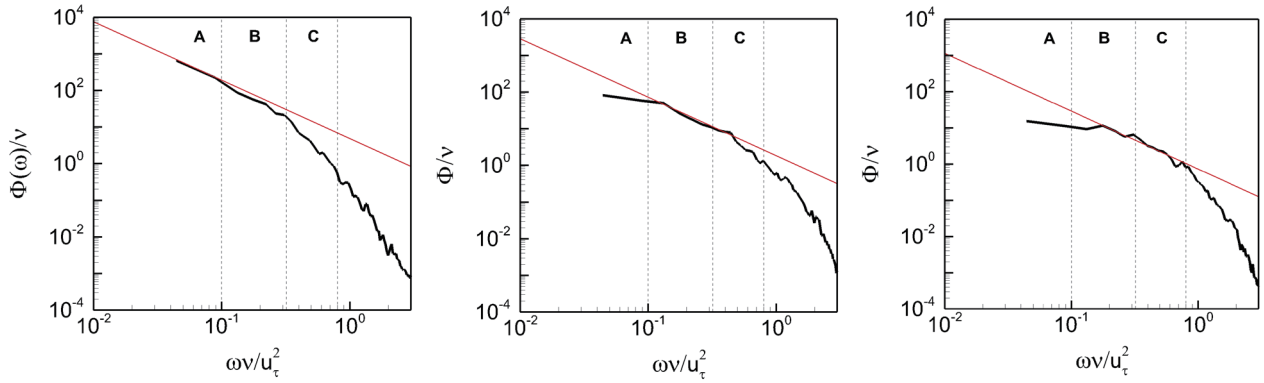

Fig. 9. Power spectra of u_z' at y^+ = 15, 70, and 150; red line: acoustic decaying slope ($f^{-8/5}$).

Haj-Hariri[18], similar to elastodynamics in terms of mode conversion from shear waves to dilatational waves.

The constant decaying rate of $f^{-8/5}$ in the power spectrum implicates a noise generation mechanism in turbulent pipe flow. It can also be interpreted in the context of dipole sound via vortex-scattering. For example, the constant decaying rate of f^{-2} of the trailing-edge noise in the power spectrum[19] is related to edge-scattering of the convecting turbulent eddies, to be more specific, the spanwise rollers (e.g. hairpin heads and their mergers). The far-field acoustic pressure is then estimated by

$$p_a' \propto \rho_\infty l(\omega_z U_c) \tag{10}$$

where l represents the associated length-scale (e.g. diameter of the spanwise roller), U_c corresponds to the eddy convection speed, and $(\omega_z U_c)$ is a vertical component of the Lamb acceleration vector, $\vec{L} = \vec{\omega} \times \vec{v}$. Assuming that ω_z is approximately constant regardless of l and with Taylor's hypothesis (l·f ~ U_c), it reads

$$p_a' \propto f^{-1} \tag{11}$$

and the acoustic power spectral density $[p_a']^2$ thereby decays as f^{-2}.

The power spectrum of turbulent pipe flow noise exhibits a similar decaying rate, $f^{-8/5}$. In this case, the spectral decaying rate is closely related to turbulent bursts of convecting longitudinal structures such as hairpin vortex and their merged structures (e.g. hairpin packets). The far-field acoustic pressure is then expressed as

$$p_a' \propto \rho_\infty l^\beta \left(\frac{\partial u_z}{\partial t}\right) \tag{12}$$

where l denotes the associated longitudinal length scale, β ≃ 1, and $(\partial u_z/\partial_t)$ is the local rate of change of the streamwise velocity. Assuming that $(\partial u_z/\partial_t)$ is approximately constant regardless of l and with the Taylor's hypothesis, the acoustic pressure reads

$$p_a' \propto f^{-\beta} \tag{13}$$

and thus $[p_a']^2 \propto f^{-2\beta}$. Note that in the present turbulent pipe flow case, β = 4/5 and thus $[p_a']^2 \propto f^{-8/5}$. β being departed from 1 may be associated with the turbulent boundary layer characteristics. The measured external TBL noise spectrum[20] shows almost the same decaying rate.

Acoustic estimation for the turbulent pipe flow is re-examined with the axial velocity fluctuation spectra presented in Fig. 9. If the sound is produced by the local rate of changes of the streamwise momentum, the velocity fluctuation power spectra, in particular, $[u_z']^2$ is expected to show the same decaying slopes across the turbulent boundary layer. The spectral decaying similarity of $f^{-8/5}$ can be found indeed in the spectra at y^+ = 15, 70, and 150, representing the layers from buffer layer, log-law layer (mid), and log-law layer (upper), respectively.

If the frequency is divided into three regimes, A ($0.04 < \omega^+ < 0.1$), B ($0.1 < \omega^+ < 0.3$), and C ($0.3 < \omega^+ < 0.8$) and with the Taylor's hypothesis used, the longitudinal wavenumbers, $A_k(0.6 < k_xR < 1.5)$, $B_k(1.5 < k_xR < 4.5)$, and $C_k(4.5 < k_xR < 12)$ correspond to the frequency ranges A, B, and C, respectively. From this, it can be configured that the turbulent pipe flow noise is generated across the boundary layer but the long waves ($0.6 < k_xR < 1.5$) are mostly generated in the buffer layer or below, while the short waves ($4.5 < k_xR < 12$) are in the upper logarithmic layer.

5. Conclusions

Aeroacoustic computation of a fully-developed turbulent

pipe flow at Re_τ = 175 and M = 0.1 was successfully conducted by an elaborate LES/LPCE hybrid computational methodology. The turbulent statistics within the pipe, i.e. inner-scaled mean velocity profile, three components of turbulence intensity, $u'_{z,rms}$, $u'_{\theta,rms}$, $u'_{r,rms}$, and turbulent shear stress are well compared with the existing DNS solutions. In regard to acoustic wave propagation in the pipe, a (1,0) higher duct mode was found by a phase angle analysis. A constant decaying rate of $f^{-8/5}$ in the acoustic power spectrum, from low to mid frequencies ($0.04 < \omega^+ < 0.4$) implicates a noise generation mechanism in turbulent pipe flow; turbulent pipe flow noise is majorly generated by turbulent bursts of correlated longitudinal structures such as hairpin vortex and their merged structures (or hairpin packets). The power spectra of the streamwise velocity fluctuations across the turbulent boundary layer indicate that the most intensive noise at $\omega^+ < 0.1$ is produced in the buffer layer with fluctuations of the longitudinal structures ($k_x R < 1.5$).

Acknowledgement

This work was supported by KISTI Supercomputing Center, Daejun, Korea under the HPC Applied Research Supporting Program (No. KSC-2013-G2-004). The authors would like to thank their support and consideration.

References

[1] Craig, R., "Flight Deck Noise Reduction", *Boeing Commercial Airplanes Breakout Session*, May 2004.

[2] Williams, J. E. F., "Surface Pressure Fluctuations Induced by Boundary Layer Flow at Finite Mach Number", *Journal of Fluid Mechanics*, Vol. 22, 1965, pp. 507-519.

[3] Arguillat, B., Ricot, D., Bailly, C. and Robert, G., "Measured Wavenumber: Frequency Spectrum Associated with Acoustic and Aerodynamic Wall Pressure Fluctuations", *Journal of Acoustical Society of America*, Vol. 128, No. 4, 2010, pp. 1647-1655.

[4] Hu, Z. W., Morfey, C. L. and Sandham, N. D., "Sound Radiation in Turbulent Channel Flows", *Journal of Fluid Mechanics*, Vol. 475, 2003, pp. 269-302.

[5] Morfey, C. L., "Amplification of Aerodynamic Noise by Convected Flow Inhomogeneities", *Journal of Sound and Vibration*, Vol. 31, 1973, pp. 391-397.

[6] Hardin, J. C. and Pope, D. S., "An Acoust/Viscous Splitting Technique for Computational Aeroacoustics", *Theoretical Computational Fluid Dynamics*, Vol. 6, 1994, pp. 323-340.

[7] Seo, J. H. and Moon, Y. J., "Linearized Perturbed Compressible Equations for Low Mach Number Aeroacoustics", *Journal of Computational Physics*, Vol. 218, 2006, pp. 702-719.

[8] Lele, S. K., "Compact Finite Difference Schemes with Spectral like Resolution", *Journal of Computational Physics*, Vol. 103, 1992, pp. 16-42.

[9] Gaitonde, D., Shang, J. S. and Young, J. L., "Practical Aspects of High Order Numerical Schemes for Wave Propagation Phenomena", *International Journal for Numerical Methods in Engineering*, Vol. 45, 1992, pp. 1849-1869.

[10] Edgar, N. B. and Visbal, M. R., "A General Buffer Zone Type Non-Reflecting Boundary Condition for Computational Aeroacoustics", *AIAA Paper* 3240, 2003.

[11] Kim, K. C. and Adrian, R. J., "Very Large-Scale Motion in the Outer Layer", *Physics of Fluids*, Vol. 11, No. 2, 1999, pp. 417-422.

[12] Townsend, A. A., *The turbulent boundary layer*, in Boundary layer Research, edited by H. Gortler, Springer-Verlag, Berlin, Vol. 1, 1958.

[13] Chin, C., Ooi, A. S. H., Marusic, I. and Blackburn, H. M., "The Influence of Pipe Length on Turbulence Statistics Computed from Direct Numerical Simulation Data", *Physics of Fluids*, Vol. 22, No. 11, 2010, 115107.

[14] Khoury, G. K. E., Schlatter, P., Noorani, A., Fischer, P. F., Brethouwer, G. and Johansson, A. V., "Direct Numerical Simulation of Turbulent Pipe Flow at Moderately High Reynolds Numbers", *Flow Turbulence Combustion*, Vol. 91, 2013, pp. 475-495.

[15] Gloerfelt, X. and Berland, J., "Turbulent Boundary Layer Noise: Direct Radiation at Mach Number 0.5", *Journal of Fluid Mechanics*, Vol. 723, 2013, pp. 318-351.

[16] Moon, Y. J., "Sound of Fluids at Low Mach Numbers", *European Journal of Mechanics-B/Fluids*, Vol. 40, 2013, pp. 50-63.

[17] Jacobson, F., "Propagation of Sound Waves in Ducts", *Note no* 31260, 2011.

[18] Herbert, K., Leehey, P. and Haj-hariri, H., "On the Mach- and Reynolds-Number Dependence of the Flat-Plate Turbulent Boundary Layer Wall-Pressure Spectrum", *Theoretical and computational fluid dynamics*, Vol. 13, 1999, pp. 33-56.

[19] Brooks, T. F. and Hodgson, T. H., "Trailing Edge Noise Prediction from Measured Surface Pressures", *Journal of Sound and Vibration*, Vol. 78, No. 1, 1981, pp. 69-117.

[20] Laufer, J., "Some Statistical Properties of the Pressure Field Radiated by a Turbulent Boundary Layer", *Physics of Fluids*, Vol. 7, No. 8, 1964, pp. 1191- 1197.